

Rheology of moderated dilute suspensions of star colloids: the shape factor

F. Balboa Usabiaga¹ and M. Ellero^{1,2,3}

¹*BCAM - Basque Center for Applied Mathematics, Alameda de Mazarredo 14, E48009 Bilbao, Basque Country - Spain*

²*Ikerbasque, Basque Foundation for Science, Calle de Maria Diaz de Haro 3, E48013 Bilbao, Basque Country - Spain*

³*Zienkiewicz Center for Computational Engineering (ZCCE), Swansea University, Bay Campus, Swansea SA1 8EN, UK*

Star colloids are rigid particles with long and slender arms connected to a central core. We show numerically that the colloid shapes control the rheology of their suspensions. In particular, colloids with curved arms and *hooks* can entangle with neighbor particles and form large clusters that can sustain high stresses. When a large cluster permeates the whole system the viscosity increases many fold. Contrary to the case of spherical colloids we observe that these effects are very strong even at moderate volumes fraction over a wide range of Péclet numbers.

I. INTRODUCTION

The rheology of colloidal suspensions has been studied extensively for spherical particles^{1–6}. The case of non-spherical colloidal suspensions has also been studied for relatively simple shapes such as ellipsoids and fibers⁷ or spheres with roughness^{8,9}. The experimental work date back, at least, to the 1940s when Lauffer employed tobacco viruses to study the rheology of suspension of rod-like colloids. For rod-like colloids the viscosity increases with the colloidal aspect ratio and for very dilute suspensions the viscosity can be significantly larger than for suspension of spherical colloids at the same volume fraction¹⁰. The stress generated in dilute suspensions of axisymmetric particles such as spheroids and fibers was studied by Brenner who gave explicit analytical expressions¹¹. Such axisymmetric colloids generate stresses that depend on their orientation which in turn introduce viscoelasticity effects even in suspensions with a Newtonian matrix and show a strong shear thinning^{11,12}. The rheology of non-spherical colloids has also been studied computationally for colloids with relatively simple shapes such as platelets^{13–15}, spheroidal particles^{16,17} or dimeric colloids¹⁸.

However, many applications and natural systems contain colloids with more complex shapes. For example, marine snow is formed by a complex aggregate of organic particles which can range from globular to rod-like particles and even long filaments and sheets^{19,20}. The interactions and entanglement between such particles can affect the aggregates rheology, cohesion and dynamics^{21–23}. Another example is aluminum alloy melts where iron impurities form complex-shaped colloids that intertwine into clusters that contaminate the alloys and can worsen their mechanical properties²⁴. Additionally, complex-shaped colloids can now be carefully synthesized thanks to the new developments in colloidal science. For example, SiO₂ can be grown over a colloidal hematite to design colloids with diverse shapes such as cubes or peanut-like shells²⁵. Controlled polymerization over a seed and further treatment of the colloids can produce diverse shapes such as dumbbells, barrels or spheres with concavities²⁵.

Photolithography has also been used to synthesize plane colloids of diverse shapes with high accuracy²⁶. Further treatment of such colloids can produce even more complex shapes such as Janus particles with tree-like shapes with thin and elongated branches²⁷. Another fabrication approach is the controlled aggregation of smaller colloids to form, for example, plane star shape colloids²⁸ or amorphous aggregates with slender arms²⁹.

Complex-shaped colloids have distinct interactions that can affect their rheology. For example, cubic colloids show a strong shear thickening at steady and oscillatory flows as their lubrication forces are stronger than the ones between spherical colloids^{30,31}. Bourrienne et al. found that suspensions of amorphous colloids formed by the aggregation of small spherical silica particles yield continuous and discontinuous shear thickening (CST and DST) at volume fractions as low as $\phi \sim 10\%$ ²⁹. Bourrienne et al. showed that the DST was controlled by the levels of hydrogen bonding interactions between colloids²⁹. A result that can be cast into the frictional model introduced by Seto et al. to explain DST in suspensions of spherical colloids^{32,33}.

Here, we study the rheology of a suspension of star colloids, also called Czech hedgehog colloids, which are formed by slender arms connected to a central core³⁴. They can be seen as an idealization of the amorphous colloids used in some experiments like the ones of Bourrienne et al²⁹. However, we do not include any friction model to incorporate the hydrogen bonds between colloids. Instead, we focus on the role of the colloidal morphology in the suspension viscosity. We find that the viscosity increases dramatically with the volume fraction and that the suspensions show shear thinning at moderate Péclet numbers (Pe). Moreover, we observe that the viscosity depends strongly on the colloidal shape, thus, the shape could be seen as a new knob to control the rheology of colloidal suspension.

The rest of the paper is organized as follows. In Sec. II we describe the model used to simulate colloidal suspensions and the morphology of star colloids. In Sec. III we describe our protocol to measure the suspension viscosity and our results. We show that the suspensions of

star colloids show large viscosities at moderate volume fractions and that the shape of the colloids control the viscosity growth with volume fraction. In particular we show that colloids with curved arms or *hooks* can entangle with nearby colloids to generate a network that resist stresses. We also study the viscosity dependence with the shear rate and observe shear thinning at moderate Pe numbers. We finish with conclusions in Sec. IV and some numerical details in the A.

II. MODEL DESCRIPTION

We simulate a Brownian suspension with N colloids immersed in a Newtonian fluid. The colloids have complex shapes as shown in Fig. 1 (Multimedia available online).

Each colloid has four arms that extend from the center to the vertices of a tetrahedron. The arms end with a *hook* shaped as a circular arc. In this work we consider four colloid models where only the size of the hooks is varied. The hooks subtend an angle $\theta = 0^\circ$ (no hook), 110° , 150° and 180° in each of the four models and the colloidal diameters are $d = 0.39, 0.69, 0.71$ and $0.71 \mu\text{m}$ respectively. For simplicity, in this work all the hooks have the same relative orientation as shown in Fig. 1. The size of the hooks controls the rheology of the suspension as it will be shown later. At small Reynolds numbers the flow is governed by the Stokes equations^{35,36}

$$-\nabla p + \eta_0 \nabla^2 \mathbf{v} = \sqrt{\frac{2\eta_0 k_B T}{\Delta t}} \nabla \cdot \mathcal{W}^n, \quad (1)$$

$$\nabla \cdot \mathbf{v} = 0, \quad (2)$$

where η_0 is the solvent viscosity and \mathbf{v} and p the flow velocity and pressure. The term on the right hand side of (1) introduces the thermal fluctuations acting during the time step n of size Δt ³⁷⁻³⁹. The fluctuations increase with the thermal energy, $k_B T$, and are delta correlated in space and time

$$\langle \mathcal{W}_{ij}^n(\mathbf{x}) \mathcal{W}_{kl}^m(\mathbf{x}') \rangle = \delta_{nm} (\delta_{ik} \delta_{jl} + \delta_{il} \delta_{jk}) \delta(\mathbf{x} - \mathbf{x}'). \quad (3)$$

At the colloids surfaces the flow obeys the no slip condition³⁶

$$\mathbf{v}(\mathbf{r}) = \mathbf{u}_p + \boldsymbol{\omega}_p \times (\mathbf{r} - \mathbf{q}_p) \text{ for } \mathbf{r} \in \text{surface colloid } p, \quad (4)$$

where \mathbf{u}_p and $\boldsymbol{\omega}_p$ are the linear and angular velocities of colloid p and \mathbf{q}_p its center. Additionally, we impose a background linear shear flow, which is equivalent to the boundary condition $\mathbf{v}(\mathbf{x}) = \mathbf{v}_0(\mathbf{x}) = \dot{\gamma}_0 z \hat{\mathbf{e}}_x$ at infinity, where $\dot{\gamma}_0$ is the imposed shear rate. The equations are closed with the balance of force and torque for each

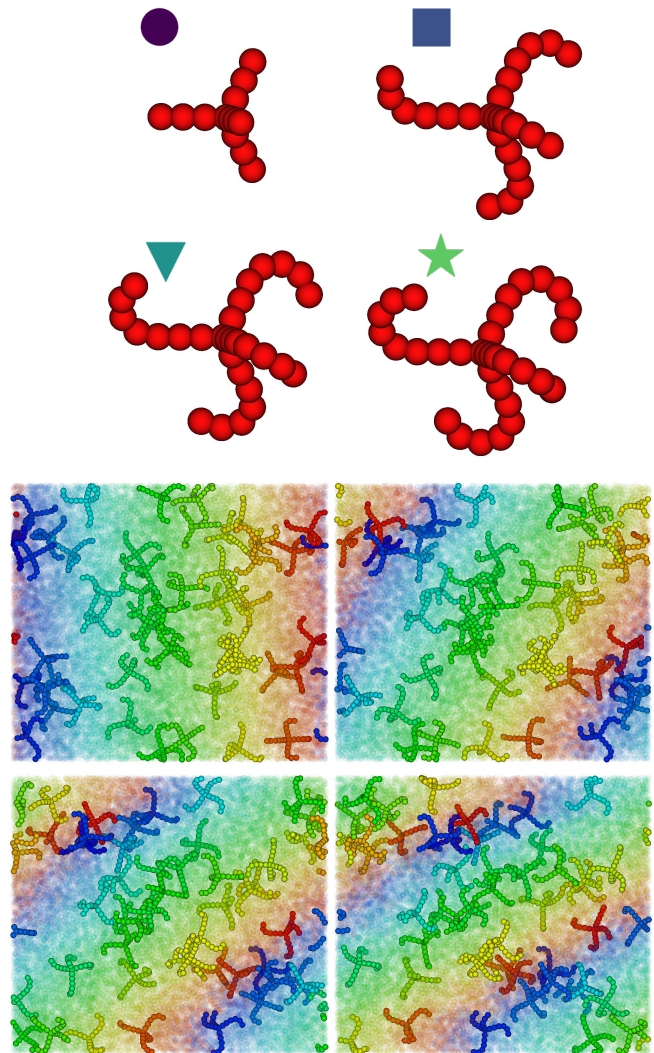


FIG. 1. **(Top)** Star colloid models used in this study and the symbols used to label their results in the rest of the paper. The colloids have four arms ending with hooks of different lengths. Their diameters (maximum distance between arms) go from $d = 0.39 \mu\text{m}$ for the first model to $d = 0.71 \mu\text{m}$ for the fourth model. **(Bottom)** Snapshots of a suspension under a linear shear flow at volume fraction $\phi = 0.2$ and Péclet number $Pe \approx 10$. A selected number of colloids is shown with full colors and the rest with a transparency to ease the visualization. The colloids are colored with their initial position along the x-axis to help visualize the shear motion (Multimedia view).

colloid p

$$\int_{S_p} \boldsymbol{\lambda}(\mathbf{r}) dS_r = \mathbf{f}_p, \quad (5)$$

$$\int_{S_p} (\mathbf{r} - \mathbf{q}_p) \times \boldsymbol{\lambda}(\mathbf{r}) dS_r = \boldsymbol{\tau}_p, \quad (6)$$

where the hydrodynamic traction, $-\boldsymbol{\lambda}$, exerted on the

colloids by the flow balances the non-hydrodynamic forces and torques, \mathbf{f}_p and $\boldsymbol{\tau}_p$, acting on the colloids³⁶.

The Eqs. (1)-(6) form a linear system that can be solved for the fluid and colloid velocities. The background flow is easily applied by splitting the flow velocity into a background and perturbation term $\mathbf{v} = \mathbf{v}_0 + \mathbf{v}^*$. As the background velocity obeys the Stokes equation the perturbation term can be solved using Eqs. (1)-(6) for \mathbf{v}^* with the known *slip* term $-\mathbf{v}_0$ on the right hand side of (4) and the condition $\mathbf{v}^*(\mathbf{x}) = 0$ at infinity. In principle, any numerical method to solve the Stokes equation could be used to simulate a suspension of star colloids⁴⁰. However, standard boundary integral methods are quite expensive for slender bodies as they require many quadrature points per body⁴¹. Instead, we use the rigid multiblob method, see a summary in A^{42,43}. The colloids are discretized with a small number of spherical *blobs* along the arms as shown in Fig. 1. These blobs interact hydrodynamically through a regularized Green's function of the Stokes equation, the Rotne-Prager mobility tensor^{44,45}. With this approach the long range hydrodynamics interaction are accurately captured while near hydrodynamics are only captured with a coarse-grained model that neglects lubrication⁴². Nevertheless the method is able to reproduce the viscosity of spherical colloid suspension for a properly chosen resolution, see Fig. 7. We compute the hydrodynamic interactions with a Fast Multipole Method which has a linear computational cost in the number of blobs in the system^{46,47}. With this approach we can simulate suspensions with up to 5000 star colloids in a single CPU, see Fig. 1 bottom (Multimedia available online).

We place N star colloids of the same kind in a simulation box of dimensions $L_x = L_y = 5\mu\text{m}$ and $L_z = 4.5\mu\text{m}$. We solve the Stokes equations with semi-periodic boundary conditions, i.e. we apply periodic boundary conditions in the x and y directions while the flow is unbounded in the z direction. We choose this setup because it is compatible with the background linear shear flow $\mathbf{v}_0(\mathbf{x}) = \dot{\gamma}_0 z \hat{\mathbf{e}}_x$. To apply the semi-periodic boundary conditions we rely on the Fast Multipole Method developed by Yan and Shelley⁴⁶, while to keep the colloids from diffusing to infinity along z we include a short repulsive potential with the planes $z = -L_z/2$ and $z = L_z/2$. We also introduce a purely repulsive potential between blobs. Both potentials have the same functional form

$$U(r) = \begin{cases} \frac{U_0 \delta}{\kappa} \left(1 + \frac{\kappa}{\delta} + \frac{\delta}{2\kappa}\right) - \frac{U_0 r}{\kappa} \left(1 + \frac{\delta}{\kappa} - \frac{r}{2\kappa}\right), & r < \delta, \\ U_0 \exp\left(-\frac{r-\delta}{\kappa}\right), & r \geq \delta. \end{cases} \quad (7)$$

The parameter δ is the distance when blobs start to overlap, we use $\delta = 2a$ for blob-blob interactions and $\delta = a$ for blob bounding planes interactions, where a is the blob radius. The parameters $U_0 = 2k_B T$ and $\kappa = 0.1a$ control the magnitude of the force and the decay length. These parameters only allow small overlaps between blobs while the interactions decay fast with the distance. Note that since our model does not include lubrication, it is crucial

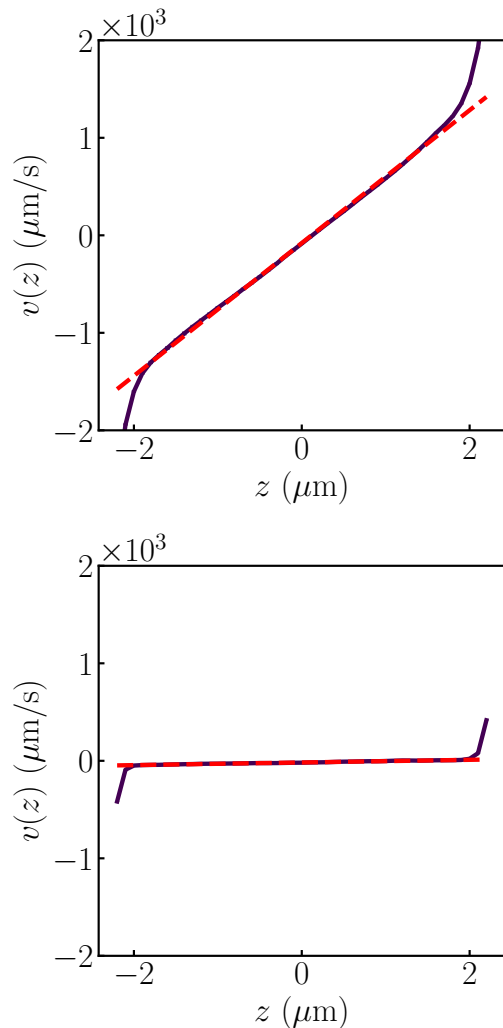


FIG. 2. Average velocity profiles (continuous lines) and fits (dashed lines) for high Péclet and volume fractions $\phi = 0.15$ and 0.25 (from top to bottom) for the model 3 of the star colloids. Away from the interfaces the velocity profiles are linear.

to include a repulsive potential between colloids.

III. RESULTS

As explained in the previous section the suspension is probed by the background shear flow $\mathbf{v}_0(\mathbf{x}) = \dot{\gamma}_0 z \hat{\mathbf{e}}_x$, with imposed shear rate $\dot{\gamma}_0$. As the colloids increase the hydrodynamic drag the velocity profile within the suspension is modified. However, it remains linear with a slope $\dot{\gamma} < \dot{\gamma}_0$ as shown in Figs. 2 and 1 bottom (Multimedia available online). This slope can be measured and used to extract the suspension viscosity. In particular, the jump in stress across the interface relates the shear rate within the suspension with its viscosity^{48,49}. Assum-

ing that the surface tension is negligible, as for colloidal suspensions^{50,51}, the jump of stress across the interface is

$$\llbracket \sigma_{xz} \rrbracket = \eta \frac{\partial v_x}{\partial z} \Big|_{\text{interface}^-} - \eta_0 \frac{\partial v_x}{\partial z} \Big|_{\text{interface}^+} = 0. \quad (8)$$

From (8) we extract the viscosity of the suspension as

$$\eta = \frac{\dot{\gamma}_0}{\dot{\gamma}} \eta_0. \quad (9)$$

We use this formula through the paper to measure the suspension viscosity for the four colloid models at different volume fractions (ϕ) and Péclet (Pe) numbers, defined here as $\text{Pe} = \dot{\gamma} d^2 / D_0$, where D_0 is the colloidal diffusion coefficient at $\phi = 0$ and d the colloidal diameter. The value of ϕ is computed with the solid volume fraction occupied by the colloids. The volume of a colloid is the volume of its blobs subtracting the small overlaps of the blobs forming the arms.

A. Viscosity versus volume fraction

First we study how the concentration and type of colloid affects the suspension viscosity at high Péclet numbers. We fix the temperature at $T = 300\text{K}$, the solvent viscosity at $\eta_0 = 10^{-3} \text{mg}/(\mu\text{m} \cdot \text{s})$, like water, the shear rate at $\dot{\gamma}_0 = 10^4 \text{s}^{-1}$ and the system size $L_x = L_y = 5 \mu\text{m}$ and $L_z = 4.5 \mu\text{m}$. With these parameters the Péclet number within the suspension is about $\text{Pe} \approx 100$. We vary the number of colloids in the computational domain to measure the viscosity from dilute suspensions, with volume fraction $\phi = 0.01$, up to moderate concentrations at $\phi = 0.30$. At the highest volume fraction our simulations have 5229 colloids for the star colloid without hooks and 2065 for the largest colloid model.

The viscosity values versus volume fraction are shown in Fig. 3 top. For the first model (no hooks) the viscosity increases faster than for spherical colloids but it only reaches moderate values, $\eta/\eta_0 \approx 19$ at $\phi = 0.30$. However, for the other models the viscosity increase is dramatic. The viscosity raises more than a hundred times for the second model and near a thousand times for the third and fourth models at the same volume fraction. In contrast, in a suspension of spherical colloids the relative viscosity only increases about a factor two at similar volume fractions, see dashed line in Fig. 3 top.

Dramatic viscosities increases as these has been observed experimentally in systems with elongated particles and friction contacts^{29,52}. However, we observe similar increases without including any friction model in the simulations. To understand the rheology we analyze the microstructure in the suspensions. First, we compute the colloidal concentration along the z -axis, see insets in Fig. 4. The confinement potential at the two planes $z = \pm L_z/2$ introduces a layering effect near them. A phenomenon observed for other suspensions near hard

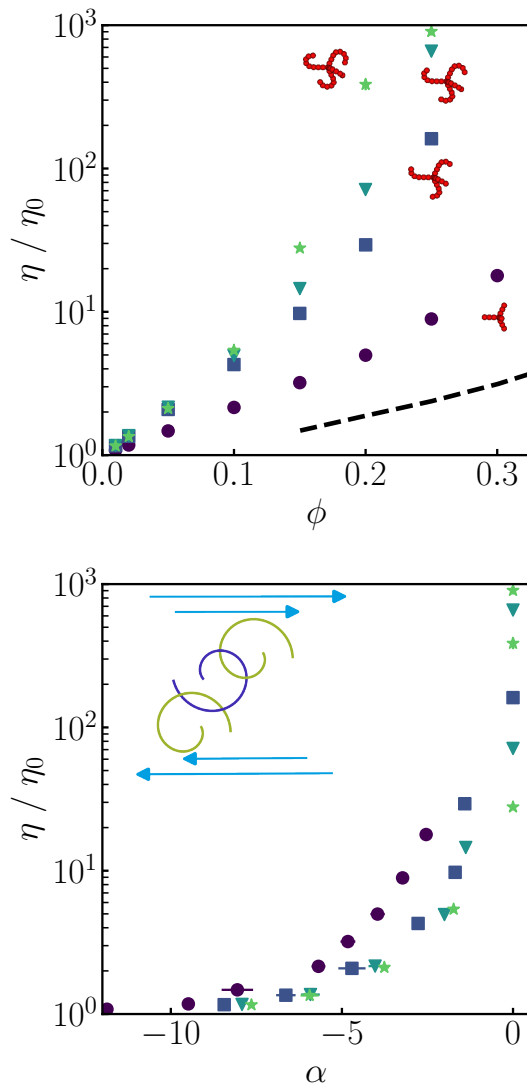


FIG. 3. **(Top)** Viscosity increase ratio η/η_0 with volume fraction ϕ for four models of star colloids at high Péclet number ($\text{Pe} \sim 100$). Colloids with curved arms or hooks show a dramatic viscosity increment at moderate volume fractions. For comparison, we show the viscosity of a suspension of spherical colloids computed by Sierou & Brady as a dashed line⁵. **(Bottom)** Viscosity versus exponent α obtained from the fit of the cluster size to a power law $P(N) \sim N^\alpha$. The inset shows a sketch of a colloidal cluster in a shear flow.

walls^{53–56}. However, away from the interface the colloidal concentration is constant and the suspensions are approximately homogeneous. Then, we analyze the microstructure within the suspension through the presence of colloidal clusters. We define a cluster as a set of colloids that are in contact, i.e. two colloids belong to the same cluster when the smallest distance between their blobs is $r_c \leq 2a$. Note that the soft repulsive potential between blobs allow small overlaps. The histograms for cluster size are shown in Fig. 4. For colloids with-

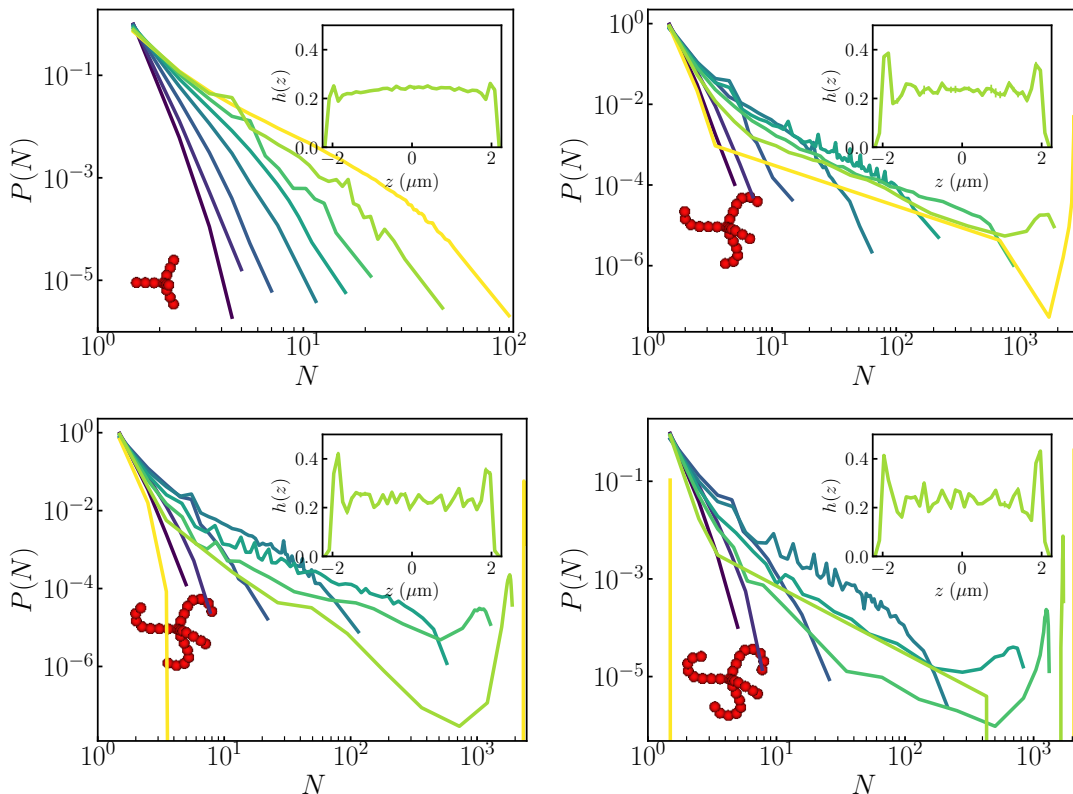


FIG. 4. Histograms of cluster size at high Péclet number for the four colloid models at volume fractions $\phi = \{0.01, 0.02, 0.05, 0.1, 0.15, 0.20, 0.25, 0.30\}$. The curve colors indicate different volume fractions raising from dilute, for dark curves, to moderate concentrations for light curves. The histogram decays like a power law, $P(N) \sim N^\alpha$, for low concentrations. When the colloids have hooks the system percolates at moderate concentrations and a single cluster span the whole system. The critical volume fraction for percolation are $\phi = 0.25, 0.2$, and 0.15 for the colloids with small, medium-sized, and large hooks respectively. Colloids without hooks, top left, do not percolate at any concentration. The insets show the concentration along the z -axis for suspensions at $\phi = 0.25$.

out hooks (first model) the number of clusters decays with size like a power law, $P(N) \sim N^\alpha$, at all concentrations. Interestingly, this is not the case for colloids with hooks. In those cases the number of cluster decays like a power law a small concentrations. However, once a critical volume fraction is reached, the system starts to percolate and a box-spanning cluster is formed. For the second colloid model this starts to happen around $\phi = 0.25$ while for the third and fourth models it occurs at $\phi = 0.20$ and $\phi = 0.15$ respectively. The formation of percolating clusters is a many body phenomena. However, the underlying mechanism for the cluster formation can be explained with a two particle system. We simulate two colloids initially entangled in a shear flow and we measure the time to disentangle. In Fig. 5 (Multimedia available online) we show that while colloids with no hooks move apart immediately, colloids with hooks can remain entangled for very long times. This phenomenon repeated over the whole suspension in many body simulations explain the different cluster size distribution for different cluster types.

To relate the presence of cluster to the suspension viscosity we fit the cluster size histograms to a power law to extract the exponent α . When a system percolates the histogram is not well fitted by a power law, thus, we simply set $\alpha = 0$ to indicate that the histogram does not decay with the cluster size. We show, for the four colloid models, the viscosity versus the exponent α in the Fig. 3 bottom. We observe an approximate collapse of the curves which indicates the important role of the cluster size on the suspension viscosity. The exponent characterizes the connectivity of the clusters within the suspension. When the colloids possess hooks they can form large clusters able to sustain large stresses which increases the viscosity. This result is similar to the large viscosity observed in suspensions where frictional contacts are active^{29,32,33,52}. In those systems the frictional, non-hydrodynamic, interactions between particles generate a network that can resist the flow very efficiently. Here we observe a similar effect generated by the colloids shape even with frictionless contacts. It seems that similar to particle models with Coulomb's friction^{32,57},

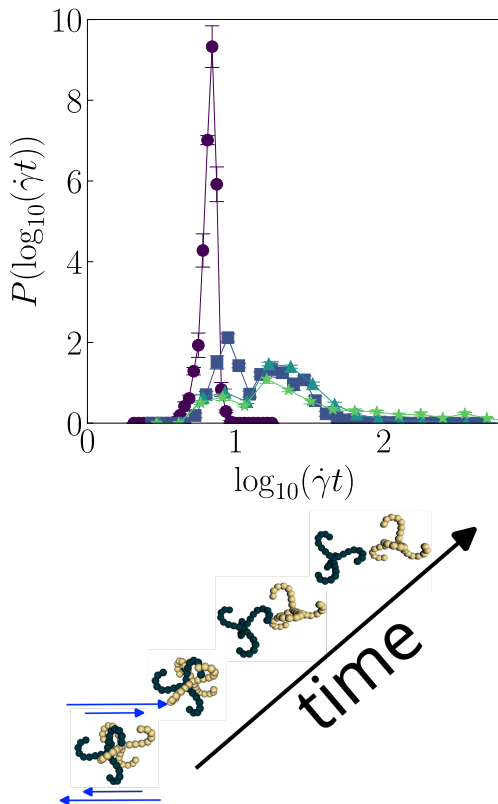


FIG. 5. **(Top)** Escape times of a two colloid cluster initially entangled with random orientations for the four colloid models represented with circles, squares, triangles and stars respectively. The results are computed for $Pe = \infty$, i.e. without thermal fluctuations using 1000 independent simulations. The presence of hooks modify completely the escape times at high Pe . **(Bottom)** Snapshots of a cluster rotating in a shear flow (blue arrows) and eventually breaking apart (Multimedia view).

irregular shapes inhibit relative motion providing additional constraints and frustrating the system. This is also similar to the model of Jamali & Brady where *explicit roughness* of frictionless spheres was shown to lead to enhanced viscosities⁵⁸.

The physical mechanism is sketched in the inset in Fig. 3 bottom. The shear flow tries to rotate the central colloid but the links to neighbor clusters prevent its rotation. If the cluster is formed by just three colloids they could be rotated by the flow. However, if they are part of a cluster that percolate the system they will not be able to rotate and will sustain a high stress which we measure as an increase in the viscosity.

B. Viscosity versus Péclet number

Once established the viscosity growth with the volume fraction we focus on the viscosity dependence with

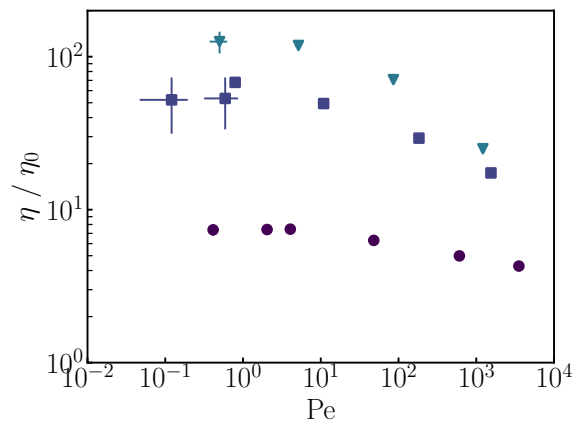


FIG. 6. Viscosity versus Péclet number for three models of star colloids. For high Pe the viscosity show shear thinning and a plateau at low Pe numbers.

the shear rate. These simulations can be very expensive as there can be a large separation of time scales between the steric and the shear time. The steric time, $\tau_{steric} = \kappa/v = \kappa^2/(\mu U_0)$, depends on the steric potential characteristic length, κ , and a typical velocity that can be estimated as $v = \mu U_0/\kappa$ where μ is the mobility of a single colloid and U_0/κ the typical force between colloids. This time scale should be short enough to avoid the crossing between blobs at large shear rates, i.e. $\tau_{steric} < \tau_{\dot{\gamma}} = 1/\dot{\gamma}$ for all shear rates. Thus, the time scale separation grows as the imposed shear rate is reduced. In order to reduce the computational cost of the simulations we exclude from this set of simulations the colloidal model with the largest hooks and, we focus on the other three models. We fix the volume fraction at $\phi = 0.2$ and vary the imposed background shear rate, $\dot{\gamma}_0$, while keeping the other parameters constant. We explore Péclet numbers in the range $Pe \approx (10^{-1} - 5 \cdot 10^3)$.

The viscosity values are shown in Fig. 6. At high Pe the viscosity shows a clear shear thinning for all the models considered while at low shear rates the viscosity reaches a plateau. The shear thinning is explained by a combination of factors. First, we include a soft repulsive potential between colloids which has been shown to introduce a shear thinning on suspensions of spherical colloids^{59–61}. As the colloids repel each other the effective free space for them is lower. However, this excluded volume depends on the shear pushing the colloids against each other. Higher shear rates can overcome the steric repulsion which increases the volume accessible to the colloids and thus reduces the *effective* volume fraction occupied by the colloids and thus the viscosity^{62,63}. Second, the Brownian motion contribution to the viscosity decreases with the Pe number, since when the time scales associated with the flow are shorter than the Brownian ones, the thermal motions cannot generate deformations that contribute to the stress and thus the viscosity^{4,64,65}. Fi-

nally, two mechanisms that counter shear thinning, leading to shear thickening, are the lubrication interaction between colloids⁴ and frictional interactions^{32,62}. However, as we explained in Sec. II our numerical method does not include lubrication nor explicit frictional interactions and thus these competing mechanism to the shear thinning are not present in our numerical results. Interestingly, the shear thinning is more pronounced for colloids with hooks than for the simpler straight star colloids as shown in Fig. 6. Similar shear thinning results were found for suspensions of Czech hedgehog colloids, star colloids without hooks, by Westwood et al., who used a close related numerical method³⁴. However, here the presence of the hooks enhance the suspension viscosity dramatically over a wide range of Pe numbers.

In the work of Bourriane et al. also strong thinning was reported in non-frictional (hydrophobic) fumed silica particles, where the presence of a yield stress was discovered²⁹. The later phenomenon was hypothesised to be connected to the presence of a percolating cluster at low Pe which is compatible with the present study. This could be another contributing factor to the thinning reported here. However, to clearly verify its nature a small amplitude oscillatory (SAOS) study should be done to check elastic versus viscous contributions to the stress which will be done in a future work.

IV. CONCLUSIONS

We have established through numerical simulations that suspensions of star colloids have extremely large viscosities even at moderate volume fractions. The relative viscosity can increase up to a factor 1000 at a volume fraction of $\phi = 0.25$ in these suspensions while with spherical colloids the relative viscosity only doubles at similar volume fractions. A cluster analysis reveals that the viscosity increases when colloids form large clusters that can resist stresses. The results in Fig. 3 show that the viscosity is correlated with the cluster size through the exponent α of the probability distribution function, $P(N) \sim N^\alpha$, of the cluster sizes. The largest viscosities are observed for $\alpha \approx 0$, when most colloids form a single cluster that spans the whole domain.

The formation of clusters is controlled by the volume fraction and, importantly, the colloid shape. Colloids with hooks can entangle with their neighbors which favors the formation of large clusters. Theoretical and experimental works have shown that the viscosity in colloidal suspensions can be enhanced by introducing friction contacts between colloids^{9,29,32,33}. Here we show that a similar enhancement can be controlled by the colloid shape instead of by their surface chemistry interactions.

In particular, we have shown that the rheology of colloidal suspensions can be affected by small changes in the colloid shape. Hooked colloids lead to much larger viscosity increases and, additionally, to a stronger shear thin-

ning. This is relevant now that complex-shaped colloids can be designed and synthesized with an array of methods. Combining the colloidal geometry with their surface chemistry would allow to design colloids that show different shear thinning or thickening effects at different shear regimes. Finally, star colloids can be chiral, i.e. they may not be symmetric under reflections. The chirality of the colloids could affect their rheology as flowing in some directions or under some drives could be easier than under others. It could be explored if this is the case and how it can be exploited to explore new physics in passive suspensions⁶⁶.

ACKNOWLEDGMENTS

The project that gave rise to these results received the support of a fellowship from “la Caixa” Foundation (ID 100010434), fellowship LCF/BQ/PI20/11760014, and from the European Union’s Horizon 2020 research and innovation programme under the Marie Skłodowska-Curie grant agreement No 847648. Funding provided by the Basque Government through the BERC 2022-2025 program and by the Ministry of Science and Innovation: BCAM Severo Ochoa accreditation CEX2021-001142-S/MICIN/AEI/10.13039/501100011033 and the project PID2020-117080RB-C55 “Microscopic foundations of soft matter experiments: computational nanohydrodynamics (Compu-Nano-Hydro)” are also acknowledged.

DATA AVAILABILITY

The data that support the findings of this study are available from the corresponding author upon reasonable request.

Appendix A: The rigid multiblob method

We delineate here the rigid multiblob method while a detailed description can be found in Ref.⁴². Colloids are discretized by a finite number of markers, or blobs, on its surface, see Figs. 1 and 7. Then, the integrals on the balance of force and torque, Eqs. (5)-(6), become sums over the blobs

$$\sum_{i \in \text{colloid } p} \boldsymbol{\lambda}_i = \mathbf{f}_p, \quad (\text{A1})$$

$$\sum_{i \in \text{colloid } p} (\mathbf{r}_i - \mathbf{q}_p) \times \boldsymbol{\lambda}_i = \boldsymbol{\tau}_p. \quad (\text{A2})$$

Here $\boldsymbol{\lambda}_i$ is the force acting on the blob i to enforce the rigid motion of the colloid. The *slip* condition is evalu-

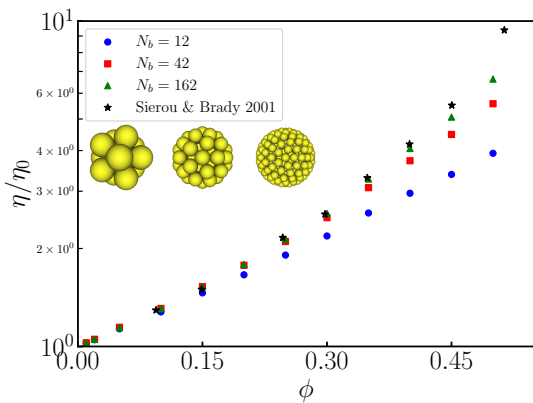


FIG. 7. Viscosity of a suspension of spherical colloids versus volume fraction. We discretize the colloids with N_b number of blobs, see insets, and compare with the results of Stokesian dynamics from Sierou & Brady⁵. The viscosity values are under predicted due to the lack of lubrication in our numerical method. The discrepancy decreases for higher resolutions.

ated at every blob i in colloid p as

$$\mathbf{v}(\mathbf{r}_i) = \sum_j \mathbf{M}_{ij} \boldsymbol{\lambda}_j = \mathbf{u}_p + \boldsymbol{\omega}_p \times (\mathbf{r}_i - \mathbf{q}_p) + \mathbf{u}_s(\mathbf{r}_i) \quad (\text{A3})$$

where the mobility \mathbf{M} couples the blobs hydrodynamically and we have included an slip term, $\mathbf{u}_s(\mathbf{r}_i)$, that we will discuss in a moment. The submatrix \mathbf{M}_{ij} computes the flow at the blob i generated by the force acting on the blob j . In boundary integral methods the mobility matrix would be the Green's function of the Stokes equation, $\mathbf{G}(\mathbf{x}, \mathbf{y})$. The rigid multiblob method uses instead a regularization of the Green's function, the so-called Rotne-Prager (RPY) mobility^{44,45}

$$\mathbf{M}_{ij} = \mathbf{M}(\mathbf{r}_i, \mathbf{r}_j) = \frac{1}{(4\pi a^2)^2} \int \delta(|\mathbf{r}' - \mathbf{r}_i| - a) \mathbf{G}(\mathbf{r}', \mathbf{r}'') \delta(|\mathbf{r}'' - \mathbf{r}_j| - a) d^3 r'' d^3 r', \quad (\text{A4})$$

which is written here as the double integral over the blobs surface. The advantage of this approach is that the RPY mobility is positive definite, which makes the scheme robust even with very low resolutions and eases the generation of the Brownian noise^{34,39,67}. The equations (A1)-(A3) form a linear system for the colloidal linear and angular velocities and the blobs constraint forces. We can write the linear system explicitly as

$$\begin{bmatrix} \mathbf{M} & -\mathbf{K} \\ -\mathbf{K}^T & \mathbf{0} \end{bmatrix} \begin{bmatrix} \boldsymbol{\lambda} \\ \mathbf{U} \end{bmatrix} = \begin{bmatrix} \mathbf{u}_s \\ -\mathbf{F} \end{bmatrix}, \quad (\text{A5})$$

with the notation $\mathbf{U} = \{\mathbf{u}_p, \boldsymbol{\omega}_p\}$, $\mathbf{F} = \{\mathbf{f}_p, \boldsymbol{\tau}_p\}$ and $\boldsymbol{\lambda} = \{\boldsymbol{\lambda}_i\}$. The geometrix matrix \mathbf{K} transform rigid body velocities to blobs velocities, thus we have used it to write the no-slip condition in (A5), i.e. $(\mathbf{K}\mathbf{U})_i =$

$\mathbf{u}_p + \boldsymbol{\omega}_p \times (\mathbf{r}_i - \mathbf{q}_p)$ for blob i . The slip term in the right hand side, $\mathbf{u}_s = -\mathbf{v}_0(\mathbf{r}) + \sqrt{2k_B T / \Delta t} \mathbf{M}^{1/2} \mathbf{W}^n$, includes the imposed background flow and the Brownian noise. In the second term \mathbf{W}^n is a vector of Gaussian noise generated at the time step n and $\mathbf{M}^{1/2}$ is the *square root* of the mobility matrix (e.g. a Cholesky factorization). This stochastic slip is equivalent to include the noise directly in the Stokes equation as in (1)^{34,39}. With the appropriate stochastic integrator the solution of this linear equation reproduces the correct Brownian motion of the colloids^{34,39}. We use the stochastic trapezoidal method described in Ref.⁴³.

To validate our numerical method we compute the viscosity of a random suspension of spherical colloids for different volume fractions. We use different resolution, i.e. number of blobs, to discretize the colloids and show the results in Fig. 7. For low volume fraction, $\phi \approx 0.15$, we get good agreement with the results of Sierou & Brady⁵ with low resolutions, for example using 12 blobs per colloid. As the concentration is increased, and the near hydrodynamic interactions gain importance, we need to use higher resolutions to recover the correct viscosity. The discrepancy can be made arbitrarily small with higher resolutions at the expense, of course, of higher computational cost. As shown in Fig. 7 the viscosities computed with the rigid multiblob method are underpredicted, which is a general feature of our approach due to the lack of lubrication interactions in the rigid multiblob method.

- ¹C. G. de Kruif, E. M. F. van Iersel, A. Vrij, and W. B. Russel, "Hard sphere colloidal dispersions: Viscosity as a function of shear rate and volume fraction," *The Journal of Chemical Physics* **83**, 4717–4725 (1985), <https://pubs.aip.org/aip/jcp/article-pdf/83/9/4717/9724633/4717.1.online.pdf>.
- ²M. Doi and S. F. Edwards, *The Theory of Polymer Dynamics* (Clarendon Press - Oxford, 1994).
- ³P. N. Segrè, S. P. Meeker, P. N. Pusey, and W. C. K. Poon, "Viscosity and structural relaxation in suspensions of hard-sphere colloids," *Phys. Rev. Lett.* **75**, 958–961 (1995).
- ⁴D. R. Foss and J. F. Brady, "Structure, diffusion and rheology of brownian suspensions by stokesian dynamics simulation," *Journal of Fluid Mechanics* **407**, 167–200 (2000).
- ⁵A. Sierou and J. F. Brady, "Accelerated stokesian dynamics simulations," *Journal of Fluid Mechanics* **448**, 115–146 (2001).
- ⁶C. D. Cwalina and N. J. Wagner, "Material properties of the shear-thickened state in concentrated near hard-sphere colloidal dispersions," *Journal of Rheology* **58**, 949–967 (2014), <https://doi.org/10.1122/1.4876935>.
- ⁷J. Mewis and N. J. Wagner, *Colloidal suspension rheology* (Cambridge university press, 2012).
- ⁸J. Y. Moon, S. Dai, L. Chang, J. S. Lee, and R. I. Tanner, "The effect of sphere roughness on the rheology of concentrated suspensions," *Journal of Non-Newtonian Fluid Mechanics* **223**, 233–239 (2015).
- ⁹R. I. Tanner and S. Dai, "Particle roughness and rheology in noncolloidal suspensions," *Journal of Rheology* **60**, 809–818 (2016), <https://pubs.aip.org/sor/jor/article-pdf/60/4/809/13986436/809.1.online.pdf>.
- ¹⁰M. A. Lauffer, "The size and shape of tobacco mosaic virus particles," *Journal of the American Chemical Society* **66**, 1188–1194 (1944).
- ¹¹H. Brenner, "Rheology of a dilute suspension of axisymmetric

- brownian particles,” *International Journal of Multiphase Flow* **1**, 195–341 (1974).
- ¹²N. Nemoto, J. L. Schrag, J. D. Ferry, and R. W. Fulton, “Infinite-dilution viscoelastic properties of tobacco mosaic virus,” *Biopolymers* **14**, 409–417 (1975), <https://onlinelibrary.wiley.com/doi/pdf/10.1002/bip.1975.360140213>.
- ¹³Q. Meng and J. J. L. Higdon, “Large scale dynamic simulation of plate-like particle suspensions. Part I: Non-Brownian simulation,” *Journal of Rheology* **52**, 1–36 (2008), https://pubs.aip.org/sor/jor/article-pdf/52/1/1/16083609/1.1_online.pdf.
- ¹⁴Q. Meng and J. J. L. Higdon, “Large scale dynamic simulation of plate-like particle suspensions. Part II: Brownian simulation,” *Journal of Rheology* **52**, 37–65 (2008), https://pubs.aip.org/sor/jor/article-pdf/52/1/37/16083179/37.1_online.pdf.
- ¹⁵T. Yamamoto and N. Kanda, “Computational model for brownian dynamics simulation of polymer/clay nanocomposites under flow,” *Journal of Non-Newtonian Fluid Mechanics* **181–182**, 1–10 (2012).
- ¹⁶E. Bertevas, X. Fan, and R. I. Tanner, “Simulation of the rheological properties of suspensions of oblate spheroidal particles in a newtonian fluid,” *Rheologica acta* **49**, 53 (2010).
- ¹⁷M. Trulsson, “Rheology and shear jamming of frictional ellipses,” *Journal of Fluid Mechanics* **849**, 718–740 (2018).
- ¹⁸R. Mari, “Shear thickening of suspensions of dimeric particles,” *Journal of Rheology* **64**, 239–254 (2020), https://pubs.aip.org/sor/jor/article-pdf/64/2/239/13922627/239.1_online.pdf.
- ¹⁹B. E. Logan and D. B. Wilkinson, “Fractal geometry of marine snow and other biological aggregates,” *Limnology and Oceanography* **35**, 130–136 (1990), <https://aslopubs.onlinelibrary.wiley.com/doi/pdf/10.4319/lo.1990.35.1.02008>.
- ²⁰A. L. Aldredge and M. W. Silver, “Characteristics, dynamics and significance of marine snow,” *Progress in Oceanography* **20**, 41–82 (1988).
- ²¹Óscar Guadayol, T. Mendonca, M. Segura-Noguera, A. J. Wright, M. Tassieri, and S. Humphries, “Microrheology reveals microscale viscosity gradients in planktonic systems,” *Proceedings of the National Academy of Sciences* **118**, e2011389118 (2021), <https://www.pnas.org/doi/pdf/10.1073/pnas.2011389118>.
- ²²Y. Song and M. J. Rau, “A novel method to study the fragmentation behavior of marine snow aggregates in controlled shear flow,” *Limnology and Oceanography: Methods* (2022), 10.1002/lom3.10509.
- ²³E. Trudnowska, L. Lacour, M. Ardyna, A. Rogge, J. O. Irsson, A. M. Waite, M. Babin, and L. Stemann, “Marine snow morphology illuminates the evolution of phytoplankton blooms and determines their subsequent vertical export,” *Nature communications* **12**, 1–13 (2021).
- ²⁴C. Caceres and J. Taylor, “Enhanced ductility in al-si-cu-mg foundry alloys with high si content,” *Metallurgical and Materials Transactions B* **37**, 897–903 (2006).
- ²⁵S. Sacanna and D. J. Pine, “Shape-anisotropic colloids: Building blocks for complex assemblies,” *Current Opinion in Colloid & Interface Science* **16**, 96–105 (2011).
- ²⁶A. Chakrabarty, F. Wang, C.-Z. Fan, K. Sun, and Q.-H. Wei, “High-precision tracking of brownian boomerang colloidal particles confined in quasi two dimensions,” *Langmuir* **29**, 14396–14402 (2013), pMID: 24171648, <http://dx.doi.org/10.1021/la403427y>.
- ²⁷B. Dai, J. Wang, Z. Xiong, X. Zhan, W. Dai, C.-C. Li, S.-P. Feng, and J. Tang, “Programmable artificial phototactic microswimmer,” *Nature Nanotechnology* (2016), 10.1038/nnano.2016.187.
- ²⁸C. P. Lapointe, K. Mayoral, and T. G. Mason, “Star colloids in nematic liquid crystals,” *Soft Matter* **9**, 7843–7854 (2013).
- ²⁹P. Bourrianne, V. Niggel, G. Polly, T. Divoux, and G. H. McKinley, “Tuning the shear thickening of suspensions through surface roughness and physico-chemical interactions,” *Phys. Rev. Research* **4**, 033062 (2022).
- ³⁰C. D. Cwalina, K. J. Harrison, and N. J. Wagner, “Rheology of cubic particles suspended in a newtonian fluid,” *Soft Matter* **12**, 4654–4665 (2016).
- ³¹C. D. Cwalina, K. J. Harrison, and N. J. Wagner, “Rheology of cubic particles in a concentrated colloidal dispersion suspending medium,” *AIChE Journal* **63**, 1091–1101 (2017), <https://aiche.onlinelibrary.wiley.com/doi/pdf/10.1002/aic.15443>.
- ³²R. Seto, R. Mari, J. F. Morris, and M. M. Denn, “Discontinuous shear thickening of frictional hard-sphere suspensions,” *Phys. Rev. Lett.* **111**, 218301 (2013).
- ³³R. Mari, R. Seto, J. F. Morris, and M. M. Denn, “Discontinuous shear thickening in brownian suspensions by dynamic simulation,” *Proceedings of the National Academy of Sciences* **112**, 15326–15330 (2015), <https://www.pnas.org/content/112/50/15326.full.pdf>.
- ³⁴T. A. Westwood, B. Delmotte, and E. E. Keaveny, “A generalised drift-correcting time integration scheme for brownian suspensions of rigid particles with arbitrary shape,” *Journal of Computational Physics* **467**, 111437 (2022).
- ³⁵S. Kim and S. J. Karrila, *Microhydrodynamics: principles and selected applications*, edited by S. K. J. Karrila (Butterworth-Heinemann, 1991).
- ³⁶C. Pozrikidis, *Boundary Integral and Singularity Methods for Linearized Viscous Flow*, Cambridge Texts in Applied Mathematics (Cambridge University Press, 1992).
- ³⁷S. Delong, F. Balboa Usabiaga, R. Delgado-Buscalioni, B. E. Griffith, and A. Donev, “Brownian dynamics without green’s functions,” *The Journal of Chemical Physics* **140**, 134110 (2014).
- ³⁸Y. Bao, M. Rachh, E. E. Keaveny, L. Greengard, and A. Donev, “A fluctuating boundary integral method for brownian suspensions,” *Journal of Computational Physics* **374**, 1094–1119 (2018).
- ³⁹B. Sprinkle, A. Donev, A. P. S. Bhalla, and N. Patankar, “Brownian dynamics of fully confined suspensions of rigid particles without green’s functions,” *The Journal of Chemical Physics* **150**, 164116 (2019), <https://doi.org/10.1063/1.5090114>.
- ⁴⁰E. Corona, L. Greengard, M. Rachh, and S. Veerapaneni, “An integral equation formulation for rigid bodies in stokes flow in three dimensions,” *Journal of Computational Physics* **332**, 504–519 (2017).
- ⁴¹L. Koens and E. Lauga, “The boundary integral formulation of stokes flows includes slender-body theory,” *Journal of Fluid Mechanics* **850**, R1 (2018).
- ⁴²F. Balboa Usabiaga, B. Kallemov, B. Delmotte, A. P. S. Bhalla, B. E. Griffith, and A. Donev, “Hydrodynamics of suspensions of passive and active rigid particles: a rigid multiblob approach,” *Communications in Applied Mathematics and Computational Science* **11**, 217–296 (2016).
- ⁴³B. Sprinkle, F. Balboa Usabiaga, N. A. Patankar, and A. Donev, “Large scale brownian dynamics of confined suspensions of rigid particles,” *The Journal of Chemical Physics* **147**, 244103 (2017), <https://doi.org/10.1063/1.5003833>.
- ⁴⁴J. Rotne and S. Prager, “Variational treatment of hydrodynamic interaction in polymers,” *Journal of Chemical Physics* **50**, 4831 (1969).
- ⁴⁵E. Wajnryb, K. A. Mizerski, P. J. Zuk, and P. Szymczak, “Generalization of the rotne-prager-yamakawa mobility and shear disturbance tensors,” *Journal of Fluid Mechanics* **731**, R3 (2013).
- ⁴⁶W. Yan and M. Shelley, “Universal image system for non-periodic and periodic stokes flows above a no-slip wall,” *Journal of Computational Physics* **375**, 263–270 (2018).
- ⁴⁷W. Yan and R. Blackwell, “Kernel aggregated fast multipole method: Efficient summation of laplace and stokes kernel functions,” arXiv (2020).
- ⁴⁸L. D. Landau and E. M. Lifshitz, *Fluid Mechanics* (Pergamon Press, Oxford, England, 1987).
- ⁴⁹Y.-N. Young, M. J. Shelley, and D. B. Stein, “The many behaviors of deformable active droplets,” *Mathematical Biosciences and Engineering* **18**, 2849–2881 (2021).

- ⁵⁰D. G. A. L. Aarts, R. P. A. Dullens, H. N. W. Lekkerkerker, D. Bonn, and R. van Roij, “Interfacial tension and wetting in colloid–polymer mixtures,” *The Journal of Chemical Physics* **120**, 1973–1980 (2004), <https://doi.org/10.1063/1.1635810>.
- ⁵¹D. G. A. L. Aarts, M. Schmidt, and H. N. W. Lekkerkerker, “Direct visual observation of thermal capillary waves,” *Science* **304**, 847 (2004).
- ⁵²A. Oseli, A. Vesel, E. Zagar, and L. S. Perse, “Mechanisms of single-walled carbon nanotube network formation and its configuration in polymer-based nanocomposites,” *Macromolecules* **54**, 3334–3346 (2021).
- ⁵³K. Yeo and M. R. Maxey, “Dynamics of concentrated suspensions of non-colloidal particles in couette flow,” *Journal of Fluid Mechanics* **649**, 205 (2010).
- ⁵⁴E. M. Fernández, E. Chacon, and P. Tarazona, “Capillary wave spectrum at adsorbed liquid films,” *Physical Review B* **86**, 085401 (2012).
- ⁵⁵X. Bian, S. Litvinov, M. Ellero, and N. J. Wagner, “Hydrodynamic shear thickening of particulate suspension under confinement,” *Journal of Non-Newtonian Fluid Mechanics* **213**, 39 – 49 (2014).
- ⁵⁶A. Vázquez-Quesada and M. Ellero, “Numerical simulations of brownian suspensions using smoothed dissipative particle dynamics: Diffusion, rheology and microstructure,” *Journal of Non-Newtonian Fluid Mechanics* **317**, 105044 (2023).
- ⁵⁷J. A. Ruiz-Lopez, S. S. Prasanna Kumar, A. Vazquez-Quesada, J. de Vicente, and M. Ellero, “Tribological variable-friction coefficient models for the simulation of dense suspensions of rough polydisperse particles,” *Journal of Rheology* **67**, 541–558 (2023), https://pubs.aip.org/sor/jor/article-pdf/67/2/541/16777835/541_1_online.pdf.
- ⁵⁸S. Jamali and J. F. Brady, “Alternative frictional model for discontinuous shear thickening of dense suspensions: Hydrodynamics,” *Phys. Rev. Lett.* **123**, 138002 (2019).
- ⁵⁹B. J. Maranzano and N. J. Wagner, “The effects of interparticle interactions and particle size on reversible shear thickening: Hard-sphere colloidal dispersions,” *Journal of Rheology* **45**, 1205–1222 (2001), https://pubs.aip.org/sor/jor/article-pdf/45/5/1205/12281501/1205_1_online.pdf.
- ⁶⁰E. Nazockdast and J. F. Morris, “Effect of repulsive interactions on structure and rheology of sheared colloidal dispersions,” *Soft Matter* **8**, 4223–4234 (2012).
- ⁶¹J. W. Swan and R. N. Zia, “Active microrheology: Fixed-velocity versus fixed-force,” *Physics of Fluids* **25**, 083303 (2013), <https://doi.org/10.1063/1.4818810>.
- ⁶²R. Mari, R. Seto, J. F. Morris, and M. M. Denn, “Shear thickening, frictionless and frictional rheologies in non-brownian suspensions,” *Journal of Rheology* **58**, 1693–1724 (2014), <https://doi.org/10.1122/1.4890747>.
- ⁶³G. Chatté, J. Comtet, A. Nigues, L. Bocquet, A. Siria, G. Ducouret, F. Lequeux, N. Lenoir, G. Ovarlez, and A. Colin, “Shear thinning in non-brownian suspensions,” *Soft matter* **14**, 879–893 (2018).
- ⁶⁴G. Bossis and J. F. Brady, “The rheology of brownian suspensions,” *The Journal of Chemical Physics* **91**, 1866–1874 (1989), <https://doi.org/10.1063/1.457091>.
- ⁶⁵J. F. Brady and J. F. Morris, “Microstructure of strongly sheared suspensions and its impact on rheology and diffusion,” *Journal of Fluid Mechanics* **348**, 103–139 (1997).
- ⁶⁶Z. Zhao, M. Yang, S. Komura, and R. Seto, “Odd viscosity in chiral passive suspensions,” *arXiv preprint arXiv:2205.11881* (2022), <https://doi.org/10.48550/arXiv.2205.11881>.
- ⁶⁷S. Delong, F. Balboa Usabiaga, and A. Donev, “Brownian dynamics of confined rigid bodies,” *The Journal of Chemical Physics* **143**, 144107 (2015).